Earthq Eng & Eng Vib (2018) 17: 325-342 **DOI**: https://doi.org/10.1007/s11803-018-0444-y

Seismic behavior of breakwaters on complex ground by numerical tests: Liquefaction and post liquefaction ground settlements

Gu Linlin[1†], Zhang Feng[2‡], Bao Xiaohua[3§], Shi Zhenming[4‡], Ye Guanlin[5‡] and Ling Xianzhang[1‡]

1. *Department of Civil Engineering, Qingdao University of Technology, Qingdao 266033, China*
2. *Department of Civil Engineering, Nagoya Institute of Technology, Nagoya 466-8555, Japan*
3. *Department of Civil Engineering, Shenzhen University, Shenzhen 518060, China*
4. *Department of Geotechnical Engineering, Tongji University, Shanghai 200092, China*
5. *Department of Civil Engineering, Shanghai Jiao Tong University, Shanghai 200030, China*

Abstract: A large number of breakwaters have been constructed along coasts to protect humans and infrastructures from tsunamis. There is a risk that foundation soils of these structures may liquefy, or partially liquefy during the earthquake preceding a tsunami, which would greatly reduce the structures' capacity to resist the tsunami. It is necessary to consider not only the soil's liquefaction behavior due to earthquake motions but also its post-liquefaction behavior because this behavior will affect the breakwater's capacity to resist an incoming tsunami. In this study, numerical tests based on a sophisticated constitutive model and a soil-water coupled finite element method are used to predict the mechanical behavior of breakwaters and the surrounding soils. Two real breakwaters subjected to two different seismic excitations are examined through numerical simulation. The simulation results show that, earthquakes affect not only the immediate behavior of breakwaters and the surrounding soils but also their long-term settlements due to post-earthquake consolidation. A soil profile with thick clayey layers beneath liquefied soil is more vulnerable to tsunami than a soil profile with only sandy layers. Therefore, quantitatively evaluating the seismic behavior of breakwaters and surrounding soils is important for the design of breakwater structures to resist tsunamis.

Keywords: breakwater; settlement; earthquake; numerical test; liquefaction

1 Introduction

Tsunamis, common disasters induced by earthquakes, pose a major threat to human society in coastal regions. It is reported that the tsunami triggered by the Great East Japan Earthquake on March 11, 2011, caused unprecedented damage to well-engineered buildings and coastal structures (Yen *et al*., 2013). Although a large number of breakwaters have been constructed along the coast to prevent tsunami-related damage, a surprisingly large number were unable to protect humans and onshore infrastructure. One of the main reasons for their failure was the liquefaction of the ground supporting the breakwaters' foundations. Because the propagation velocity of seismic excitations is greater than that of tsunamis, the ground could have been liquefied before the tsunami arrived. As noted by Wang *et al*. (2013) and Sawicki *et al*. (2009), when a breakwater sits on liquefied soils and is subjected to an earthquake, it exhibits a large settlement after excess pore water pressure (EPWP) has built up in the ground. As a result, the breakwater's ability to resist the tsunami drops significantly. Devastating damage to the breakwaters and other structures built on liquefied or partially liquefied soil were recorded in the tsunami generated by the 2011 Great East Japan Earthquake (Imase *et al*., 2012).

Unfortunately, many breakwaters have been designed without considering this type of combined loading, consisting of both earthquake motion that may cause liquefaction and tsunami loading that may cause catastrophic failure of infrastructure. Therefore, the performance of breakwaters during or after an earthquake needs to be investigated more closely. However, it is quite difficult to investigate not only the instant reaction of a breakwater subjected to a strong earthquake but

Correspondence to: Bao Xiaohua, Department of Civil Engineering, Shenzhen University, Shenzhen 518060, China
Tel: +86 755-8667-0364; Fax: +86 755-2673-2850
E-mail: bxh@szu.edu.cn
†Lecturer; ‡Professor; §Associate Professor

Supported by: National Natural Science Foundation of China under Grant Nos. 51678369, 41627801 and 41372284, Technical Innovation Foundation of Shenzhen under Grant No. JCYJ20170302143610976, Doctoral Fund of Shandong Province under Grant No. ZR2017BEE071, China Postdoctoral Science Foundation under Grant No. 2017M612227 and the Special Project Fund of Taishan Scholars of Shandong Province under Grant No. 2015-212
Received June 2, 2016; **Accepted** February 14, 2017

also the consequential long-term settlement of soft ground, including sandy and clayey soils, using physical models. Hence, numerical tests based on a sophisticated constitutive model and the soil-water coupling finite element method (FEM) could be appropriate approaches for predicting the behavior of breakwaters in this increasingly important engineering problem.

Numerical testing has the potential to become an effective tool for investigating the mechanical behavior of earth structures in geotechnical engineering. Moreover, this type of test has many advantages over ordinary experimental methods. First, the loading conditions and the ground conditions can be rapidly and efficiently changed at no extra cost. Second, numerical tests are capable of reproducing the responses of liquefied and partially liquefied soils with different densities, different loading histories and different soil layer characteristics. Of course, to makes sense, the constitutive model used in the numerical test should be able to describe the mechanical behavior of the soils subjected to different loadings under different conditions in a unified way. The aims of this study are to investigate the seismic performance of soils on which two breakwaters are laid when they are exposed to an earthquake and to examine how much the breakwater's effectiveness deteriorates after the earthquake and before the following tsunami's arrival. In the numerical test in this study, all of the soil parameters are fixed in all loading processes. The calculated results are then compared and discussed to reach useful conclusions, just as in a physical model test. As the breakwater may experience large subsidence or tilting and become unstable or damaged during a strong earthquake, so its capacity to resist a tsunami after an earthquake may greatly decrease.

It is commonly known that sandy soils can liquefy during an earthquake, while it would take a long time for the full consolidation of clayey soils after an earthquake. Recent research revealed that even if the clayey soils would not liquefy, they might lose more than half of the mean effective stress in undrained cyclic triaxial loading tests (Furuta, 2003). In addition, the clay will shrink and consequently the ground will settle after the dissipation of the EPWP. To investigate the nonlinear dynamic behavior of soils during earthquake loading, Pastor *et al*., (1990) introduced a very effective general model describing the behavior of sands and clays under monotonic or transient loading. Wang *et al*. (1990) proposed a bounding surface hypoplasticity model and investigated the nonlinear behavior of sand. Wang and Xie (2014) developed a modified bounding surface hypoplasticity model to capture distinct dilatancy behaviors of loose and dense sandy soils during various phases of undrained cyclic loading based on observations from laboratory tests. By adopting the concepts of subloading (Hashiguchi and Ueno, 1977) and superloading (Asaoka *et al*., 2002), Zhang *et al*. (2007) proposed a constitutive model which can describe the mechanical behavior of soils under different drainage and loading conditions. Because the intermediate principal stress has a great effect on the mechanical behavior of soils (Ye *et al*., 2012 and 2013), Zhang *et al*. (2011) and Ye *et al*. (2012) extended Zhang's model to describe the mechanical behavior of soils under general three-dimensional stress conditions. Based on Zhang's model, Ye *et al*. (2007) conducted a series of numerical analyses using an FEM code called DBLEAVES (Ye, 2007) to simulate shaking-table tests of a saturated sandy soil under repeated liquefaction-consolidation processes. Their numerical simulations were able to produce the responses of liquefied grounds with different densities and stress-induced anisotropies during repeated shaking and consolidation processes. In addition, the program DBLEAVES is capable of solving many geotechnical engineering problems related to static-dynamic loading under different boundary and drainage conditions for earth structures, including embankment, group-pile foundations, retaining walls *et al*. Using this program, the mechanical properties of soils and structures under static loading and dynamic loading can be accurately predicted. These capabilities showed the potential of the numerical method to describe the liquefaction or partial liquefaction of soils.

In addition to the above-mentioned works, there are many other studies (Novikova *et al*., 2007; Huang *et al*., 2010) on ground liquefaction using fully nonlinear numerical simulation methods. Huang *et al*. (2012) conducted a seismic liquefaction analysis of a reservoir dam foundation before and after anti-liquefaction treatments to confirm the effectiveness of treatments used during an earthquake. Hur *et al*. (2010) carried out numerical simulations to investigate wave-induced EPWP and flow changes inside the rubble mound of a composite breakwater and its seabed foundation. Ye *et al*. (2015 and 2016) performed nonlinear simulations to investigate the seismic dynamics of offshore breakwaters on liquefiable seabed foundation. Bao *et al*. (2016) analyzed the co-seismic and post-seismic behavior of a wall type breakwater on a natural ground composed of a liquefiable layer using soil-water fully coupling finite element method. It is, therefore, reasonable to say that numerical simulation can be used as an important tool to investigate the response of geotechnical structures.

In this study, numerical tests on two real breakwaters constructed on the seabed forty years ago are performed to evaluate the tsunami resistance capacity of existing breakwaters that were not designed based on the combined loading of the earthquake motion and tsunami.

2 Evidence for liquefaction damage to breakwaters before tsunami

Because seismic excitations propagate much faster than tsunamis, they can cause the foundation soils of breakwaters to liquefy before a tsunami arrives, making the breakwaters vulnerable. Figure 1(a) and (b) showed two different failure modes of U-shaped water irrigation

(a) Damage due to tsunami only (b) Damage due to liquefaction and tsunami

Fig. 1 Different damage patterns of U-shaped water tubes in 2011 Great East Japan Earthquake

pipes caused by ground liquefaction and tsunami generated in the 2011 Great East Japan Earthquake. Figure 1(a) is a photograph taken from the site without liquefaction while Fig. 1(b) is a photograph taken from the liquefied site nearby the site in Fig. 1(a). In Fig. 1(a), the pieces of the guide rail damaged by the tsunami scattered widely, but the water tubes remained intact because the surrounding ground did not liquefy. By contrast, as shown in Fig. 1(b), taken from the liquefied site nearby, not only was the guide rail damaged but the water tubes had floated to the surface and scattered widely; some were 100 meters away from the original site. This damage occurred because the surrounding ground had experienced severe liquefaction before the tsunami struck; the tubes floated to the surface and were washed away by the tsunami at the time about 30 minutes after earthquake loading. To properly design a breakwater placed on soft soil, it is very important to understand not only tsunami forces but also the mechanical behavior of the surrounding soil during and after an earthquake. Generally speaking, it is very difficult, though not impossible, to conduct a physical model test and examine how a breakwater reacts to earthquake motions and subsequent tsunamis. Numerical tests based on a rational and sophisticated constitutive model for soft soil, however, make it possible to assess the above-mentioned behavior.

3 Numerical tests with soil-water coupled dynamic analyses

3.1 Outline of the constitutive model for soils

The selection of a constitutive model to describe the behavior of both liquefied and partially liquefied soil is a key factor in the accuracy of the numerical analysis. In this dynamic analysis using numerical tests, soils are modeled by the Cyclic Mobility Model, a kinematic hardening elastoplastic model with an associated flow rule that was initially proposed by Zhang *et al*. (2007). The main feature of this model is its capacity to describe the static and dynamic behavior of soils by considering the effects of stress-induced anisotropy, density, and the structure formed during the natural deposition process in a unified way. A detailed description of this model can be found in Zhang *et al*. (2007 and 2011). In the model, eight parameters are employed, five of which, namely, M, N, λ, κ, and ν, are also used in the Cam-Clay model. The other three parameters (a, the parameter controlling the collapse rate of the structure; m, the parameter controlling the loss rate of the overconsolidation ratio or changes in soil density; and b_r, the parameter controlling the rate of development of the stress-induced anisotropy) have clear physical meanings and can be easily determined by undrained triaxial cyclic loading tests and drained triaxial compression tests.

This model was originally developed to describe the features of clean sands, including its cyclic mobility, liquefaction strength, stress-strain relation, and effective stress path. Nevertheless, it is also capable of describing the behavior of clayey soils. The main differences between the mechanical behavior of sands and clays are the collapse rate of structure and loss rate of overconsolidation (Asaoka, 2003). For sands, the collapse rate of the structure is the high and the loss rate of overconsolidation is low. On the contrary, for clays, the collapse rate of the structure is low, whereas the loss rate of overconsolidation is high. A detailed description of the model can be found in the work of Zhang *et al*. (2007, 2011).

3.2 Problem description

In this study, numerical tests were performed on two real breakwaters, Breakwater N and Breakwater C, constructed on the seabed and the section views of the breakwaters with their soil foundations are shown in Figs. 2 and 3, respectively. The 2D numerical analyses were conducted using the program DBLEAVES. The soil profiles for the two breakwaters, shown in Figs. 2 and 3, mainly consisted of sandy and clayey soils. Breakwater N was placed on a loose sandy layer, whereas Breakwater C was placed on a soft clayey layer. As shown in Fig. 2, the computation domain of the foundation for Breakwater N is 240 m in length and 43 m in height. From top to the bottom, the ground underneath Breakwater N consists of a loose sandy layer As, three clayey layers Ac-1, Ac-2 and Ac-3, and a dense sandy layer Ds. The thickness of each soil layer is 8 m (As), 11 m (Ac-1), 16 m (Ac-2),

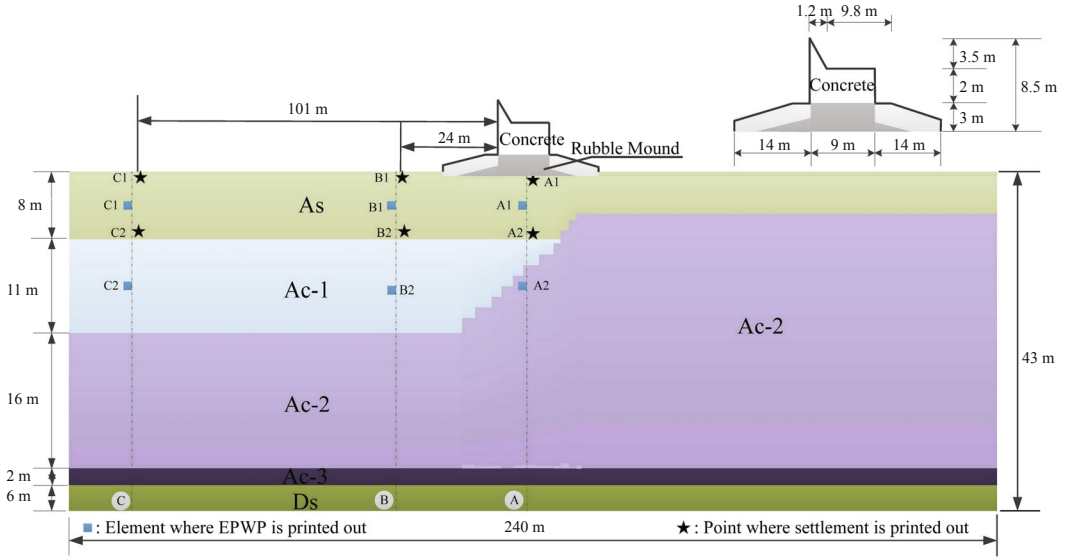

Fig. 2 Outline and soil profiles of Breakwater N

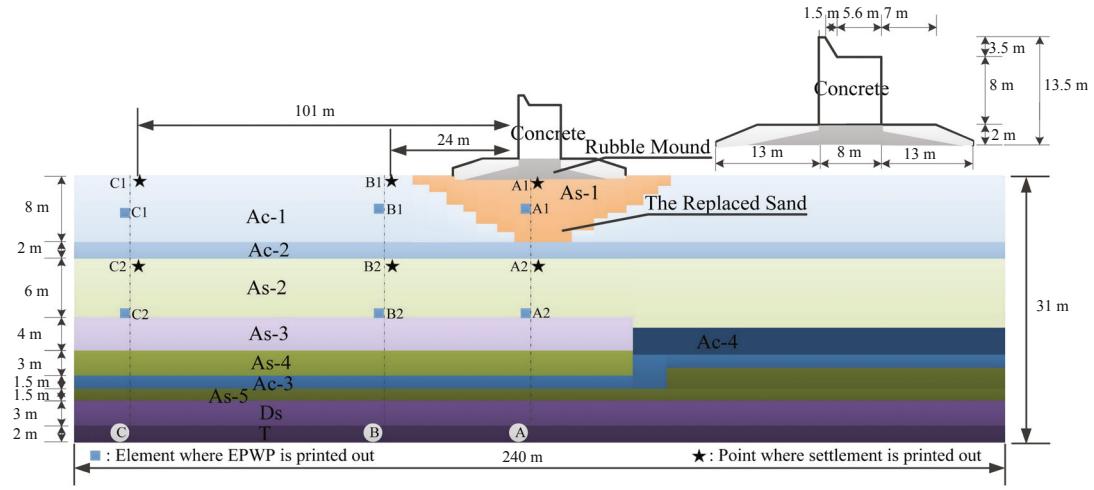

Fig. 3 Outline and soil profiles of Breakwater C

2 m (Ac-3) and 6 m (Ds). A rubble mound lies beneath the concrete caisson in Breakwater N. The size of each part of breakwater N is shown in Fig. 2, in which the total height of the breakwater is 8.5 m, while the length of the rubble mound is 37 m. The soil profile of the foundation underneath breakwater C is more complex than that underneath breakwater N. Figure 3 shows that the ground mainly consists of four clayey layers Ac-1, Ac-2, Ac-3 and Ac-4, and five sandy layers As-2, As-3, As-4, As-5 and Ds. The soil underneath the breakwater C was replaced by dense sand As-1. The soil beneath the Ds layer is the bed rock T. The thickness of each soil layer and size of the breakwater are shown in Fig. 3. It is known from past experiences that a saturated sand stratum in a shallow layer would liquefy easily and a soft clayey surface layer would deform significantly even if it does not liquefy during a strong earthquake. For this reason, even if a breakwater does not fail immediately after an earthquake, the ground settlement and the decrease in the shear resistance of foundation soils due to liquefaction or a significant reduction in the effective stress would be catastrophic for the breakwater.

In the analyses performed here, the boundary and drainage conditions of the ground were as follows: (a) the base nodes of the FE mesh were assumed to be totally fixed; (b) the nodes of two lateral sides of the computation domain with a length of 240 m were restricted by an equal-displacement condition. As the equal-displacement boundaries were assumed between the nodes on two lateral sides at the same level of the ground, the ground would shake in horizontal direction just as the case in shaking table tests when the seismic wave is applied from the base. Regarding the drainage conditions, the bottom and two lateral sides were impervious while the ground surface was assumed to be a drainage boundary. The numerical method used is an effective stress based 2D/3D soil-water coupling finite element-finite difference method based on Biot's theory

(Biot, 1941). In the analyses, the direct integration method of Newmark-β in which two parameters were introduced ($\beta = 0.3025$ and $\gamma = 0.5$) was adopted, and the time interval of the integration for dynamic loading was 0.01 sec. It is true that sometimes a smaller time interval, e.g., 0.001 sec, is needed. However, in the present case, convergent results can be obtained using the time interval of 0.01 sec. The Rayleigh type of initial rigidity proportional attenuation is used and the damping values of the soils and the structure are both assumed to be 2% and 10% for the first and second modes, respectively, in the dynamic analysis of the breakwater and foundation system. The calculation using the program DBLEAVES has been proved to be very stable in many research studies available in the literature (Bao *et al*., 2012; Bao *et al*., 2014).

3.3 Loading conditions and behavior of the soil elements

To reflect the seismic behavior of the two breakwaters and the surrounding ground during earthquakes, two earthquake waves (Sugito *et al*., 2013; http://www1.gifu-u.ac.jp/~eerl/kensaku/index.html), referred to as Case 1 and Case 2 in Fig. 4, were used as the input earthquake waves. These two waves varied greatly in duration and maximum acceleration. The earthquake motions currently used in dynamic analyses for seismic design in Japan are usually predicted on the basis of fault locations, the magnitudes and the spectra of recorded accelerograms of previous small earthquakes. This evaluation method has been authorized by the Central Disaster Management Council (CDMC). The predicted earthquake motions at any specific site are open and accessible to any seismic designer in Japan. The lengths of Case 1 and Case 2 were 200 s and 163.84 s, respectively, and the maximum accelerations of Case 1 and Case 2 were 188.00 gal and 151.49 gal, respectively. The response spectra of these two earthquake waves are shown in Fig. 4, in which h is the damping ratio. Both of these two seismic excitations were applied to Breakwater N and Breakwater C. Therefore, the four scenarios including both dynamic and static analysis shown in Table 1 were examined in the numerical tests. The difference between the static and dynamic analysis, in the viewpoint of field equation, is the existence of inertial and viscous terms. If external load is a static, then the inertial and viscous terms will automatically disappear. In the program DBLEAVES, the dynamic and static analyses are not necessary to assign. It is based on the external loads. In the analyses, crucially important, the constitutive model should be able to describe the mechanical behavior of geomaterials subjected to different loadings (static or dynamic) under

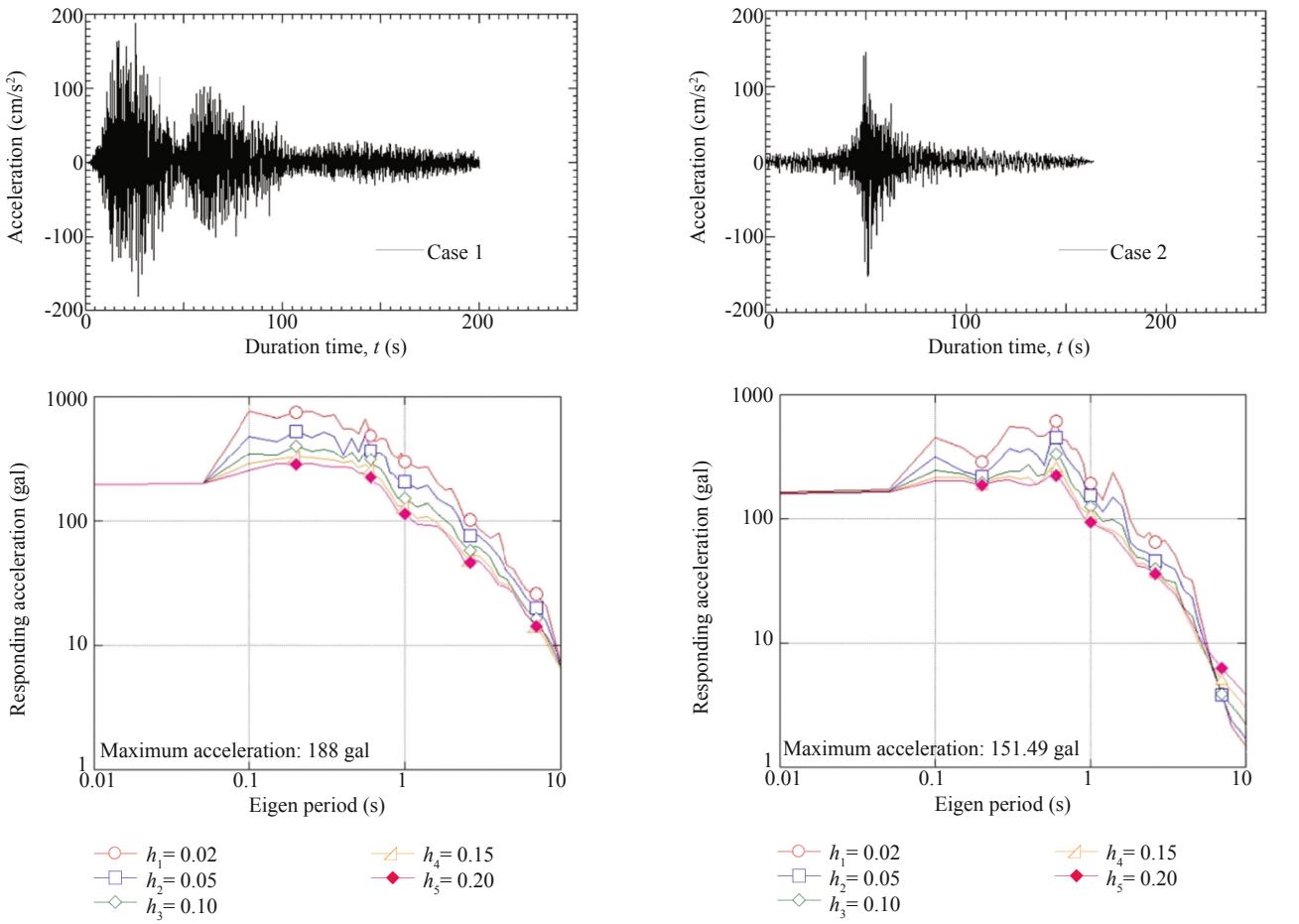

Fig. 4 Two artificial seismic waves and their response spectra

Table 1 Cases of simulation

Research condition	Breakwater name	Seismic wave
Case N-1	N	Case 1
Case N-2	N	Case 2
Case C-1	C	Case 1
Case C-2	C	Case 2

different hydraulic conditions (drained or undrained) in a unified way. The program DBLEAVES satisfies both the requirements. In the calculation, after dynamic analysis for the earthquake motion, the calculation stage automatically turns to static analysis to calculate the consolidation process (be aware of the fact that even if the earthquake motion ended, the migration of excess pore water will not stop and consolidation will then continue).

The numerical tests focused on the responses of the ground below the breakwaters' foundations during and after the earthquakes, particularly the ground settlement and changes in EPWP. In each calculation, the breakwater, made of a concrete caisson and rubble mound, was described by a linear elastic model; its parameters are shown in Table 2. The Cyclic Mobility Model (Zhang *et al*., 2007 and 2011) was used to describe the sandy and clayey soils. In this model, the parameter a is used to control the collapse rate of the structure, and the parameter m is used to control the loss rate of the overconsolidation ratio. As mentioned above, the main differences between the mechanical behavior of sands and clays are the collapse rate of the structure and loss rate of overconsolidation, so the model can be used for modeling the response of both sands and clays by different settings of parameters a and m. The material parameters and the initial values of the state parameters in the four calculations are listed in Tables 3-6. The strength and stiffness of the soil were the same as those evaluated using the Cam-Clay model, in which M represents the shear stress ratio at the critical state (i.e., it represents the strength of a soil), λ and κ represent the compression and swelling index, respectively, controlling the deformation of the soil (i.e., they are the stiffness parameters). Since not enough laboratory testing data of soils were available, some of these parameters were determined by element simulations with reference to the SPT (standard penetration tests) N-values based on engineering judgment (Morikawa *et al*., 2013). The average N-values and coefficients of permeability assumed for each soil layer beneath the Breakwaters are given in Tables 7 and 8.

Table 2 Physical properties of breakwater (Concrete)

Elastic modulus E (kPa)	2.5×10^7
Poisson's ratio v	0.20
Density ρ (t/m^3)	2.5

To verify the performance of the Cyclic Mobility Model, Fig. 5 shows the liquefaction strength curve of Toyoura sand in undrained cyclic triaxial tests, which are very familiar to seismic engineers because it is very easy for them to use the curves to estimate the seismic performance of a soil. The material parameters of Toyoura sand are listed in Table 9, which are the same as those used for Toyoura sand by Zhang *et al*. (2007, 2011).

Note that the validity of the Cyclic Mobility Model, that is, the capacity to properly describe the mechanical behavior of Toyoura sand not only subjected to monotonic loading but also cyclic loading under undrained and drained conditions, has been proved in previous research listed in the references. It is true that it is more appropriate to use cyclic triaxial test results to obtain the parameters of the soils considered. Unfortunately, up until now, only the monotonic drained triaxial test results have been available. As a compensation for this shortcoming, the undrained cyclic triaxial test results of Toyoura sand that have been obtained in previous work are used, primarily to indirectly illustrate the fact that the constitutive model is capable of describing the nonlinear dynamic behavior of soils.

In the present study, drained conventional triaxial tests of surface soil in Breakwater N and C were conducted. Undisturbed samples from As layer in Breakwater N and Ac-1 layer in Breakwater C were dug from the construction site using a thin-walled tube sampler, and they were both taken from the ground at the depth of 4 m. Drained conventional triaxial tests were carried out to investigate the stress-strain relations and dilatancy of the soils. Figure 6 shows a comparison of the results from the conventional drained triaxial tests and the corresponding element simulations of soils in the As layer and Ac-1 layer. The stress-strain relations and change of volumetric strain are on the whole, well simulated as shown in the figure, although there are still small differences between the results of tests and simulations.

Figures 7 and 8 illustrate the simulated behavior of the deviator stress-shear strain relation and the effective stress path of the soils underneath Breakwater N and Breakwater C, respectively, under undrained conventional triaxial cyclic loading tests. As shown in the figures, for loose sand (As and As-1), liquefaction occurred after five cycles of cyclic mobility, and the stiffness that was regained during cyclic loading was apparent during the loading process. For dense sand (As-5), however, although a large fraction of the effective mean stress was lost, liquefaction did not occur. The clayey soil did not liquefy while the mean effective stress decreased considerably during the cyclic loading. The clay lost up to three-fourths of its original effective stress at the end of loading. This implies that the shear strength of the clayey soil decreased dramatically when it was subjected to cyclic loading. The readers can easily image the element behavior of the soils through the

Table 3 Material parameters of soils beneath Breakwater N

Parameter	Ds	Ac-3	Ac-2	Ac-1	As
Compression index λ	0.050	0.13	0.13	0.13	0.05
Swelling index κ	0.0064	0.066	0.066	0.066	0.0064
Stress ratio of critical state M	1.42	1.24	1.24	1.21	1.41
Void ratio N (p'= 98 kPa on *N.C.L.*)	0.89	0.96	0.92	0.94	1.09
Poisson's ratio v	0.31	0.4	0.4	0.38	0.30
Degradation parameter of overconsolidation state m	0.10	2.20	2.20	2.20	0.10
Degradation parameter of structure a	2.20	0.03	0.03	0.06	2.10
Evolution parameter of anisotropy b_r	1.50	0.10	0.10	0.10	1.50

Table 4 Material parameters of soils beneath Breakwater C

Parameter	Ds	As-5	Ac-3	As-4	Ac-4	As-3	As-2	Ac-2	Ac-1	As-1
Compression index λ	0.05	0.05	0.13	0.13	0.13	0.05	0.05	0.13	0.13	0.05
Swelling index κ	0.0064	0.0064	0.066	0.066	0.066	0.0064	0.0064	0.066	0.066	0.0064
Stress ratio of critical state M	1.42	1.41	1.23	1.41	1.23	1.41	1.41	1.22	1.22	1.42
Void ratio N (p'= 98 kPa on *N.C.L.*)	0.81	0.85	0.90	0.87	0.92	0.90	0.91	0.94	0.96	0.98
Poisson's ratio ν	0.30	0.31	0.40	0.32	0.42	0.30	0.35	0.40	0.40	0.30
Degradation parameter of overconsolidation state m	0.10	0.10	2.20	0.10	2.20	0.10	0.10	2.20	2.20	0.10
Degradation parameter of structure a	2.20	2.20	0.05	2.20	0.05	2.20	2.20	0.05	0.02	2.20
Evolution parameter of anisotropy b_r	1.50	1.50	0.10	1.50	0.10	1.50	1.50	0.10	0.10	1.50

Table 5 Initial values of the state variables for soils beneath Breakwater N

Parameter	Ds	Ac-3	Ac-2	Ac-1	As
Void ratio e_0	0.79	0.89	0.90	0.92	1.10
Mean effective stress p' (kPa)	378.50	342.00	239.00	117.50	45.00
Degree of structure R_0^*	0.40	0.40	0.40	0.50	0.80
Overconsolidation OCR ($1/R_0$)	25.00	3.00	2.00	2.00	5.00
Anisotropy ζ_0	0.0	0.0	0.0	0.0	0.0

Table 6 Initial values of the state variables of soils beneath Breakwater C

Parameter	Ds	As-5	Ac-3	As-4	Ac-4	As-3	As-2	Ac-2	Ac-1	As-1
Void ratio e_0	0.80	0.83	0.89	0.86	0.91	0.92	0.91	0.96	0.97	1.01
Mean effective stress p' (kPa)	224.87	259.75	237.50	215.5	200.50	161.00	120.50	84.50	38.00	52.00
Degree of structure R_0^*	0.80	0.80	0.60	0.80	0.60	0.80	0.80	0.60	0.60	0.40
Overconsolidation OCR ($1/R_0$)	27.00	25.00	2.00	22.00	2.00	16.00	15.00	2.00	2.00	4.00
Anisotropy ζ_0	0.0	0.0	0.0	0.0	0.0	0.0	0.0	0.0	0.0	0.0

Table 7 The average *N*-values and permeability for soils beneath Breakwater N

Layer	Ds	Ac-3	Ac-2	Ac-1	As
N-value	above 50	3	2	2	5
Permeability k (m/sec)	4×10^{-4}	1×10^{-9}	1×10^{-9}	1×10^{-9}	1×10^{-4}

Table 8 The average *N*-values and permeability for soils beneath Breakwater C

Layer	Ds	As-5	Ac-3	As-4	Ac-4	As-3	As-2	Ac-2	Ac-1	As-1
N-value	above 50	20	3	13	3	13	11	2	2	15
Permeability k (m/sec)	4×10^{-4}	5×10^{-5}	1×10^{-9}	5×10^{-5}	1×10^{-9}	5×10^{-5}	5×10^{-5}	1×10^{-9}	1×10^{-9}	5×10^{-5}

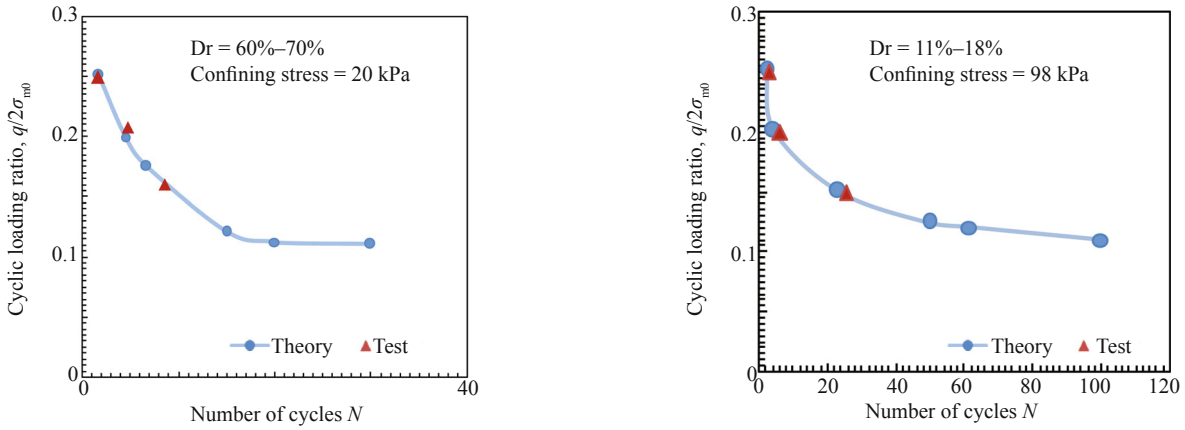

Fig. 5 Liquefaction strength curve of Toyoura sand in undrained cyclic triaxial loading

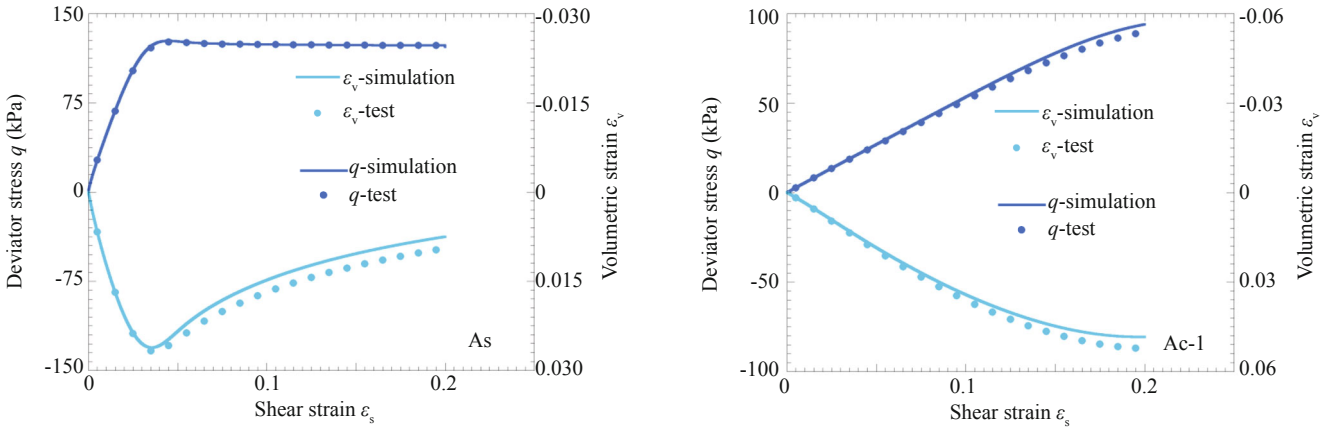

Fig. 6 Comparison between test and simulation in monotonic drained triaxial tests

Table 9 Material parameters of Toyoura sand

Compression index λ	0.050
Swelling index κ	0.0064
Principal stress ratio at critical state R_f	3.3
Void ratio N (p=98 kPa on *N.C.L.*)	1.0
Poisson's ratio v	0.30
Degradation parameter of overconsolidation state m	0.010
Degradation parameter of structure a	2.2
Evolution parameter of anisotropy b_r	1.5

simulated results.

Based on the numerical tests, physical quantities such as the ground settlement and the development of EPWP at different depths along the vertical lines A, B, and C in the cases of two breakwaters shown in Figs. 2 and 3 were graphed for discussion.

4 Results and discussions

4.1 Displacements of Breakwater N

The settlements of Breakwater N and Breakwater C during the earthquakes and sixty-eight years (time

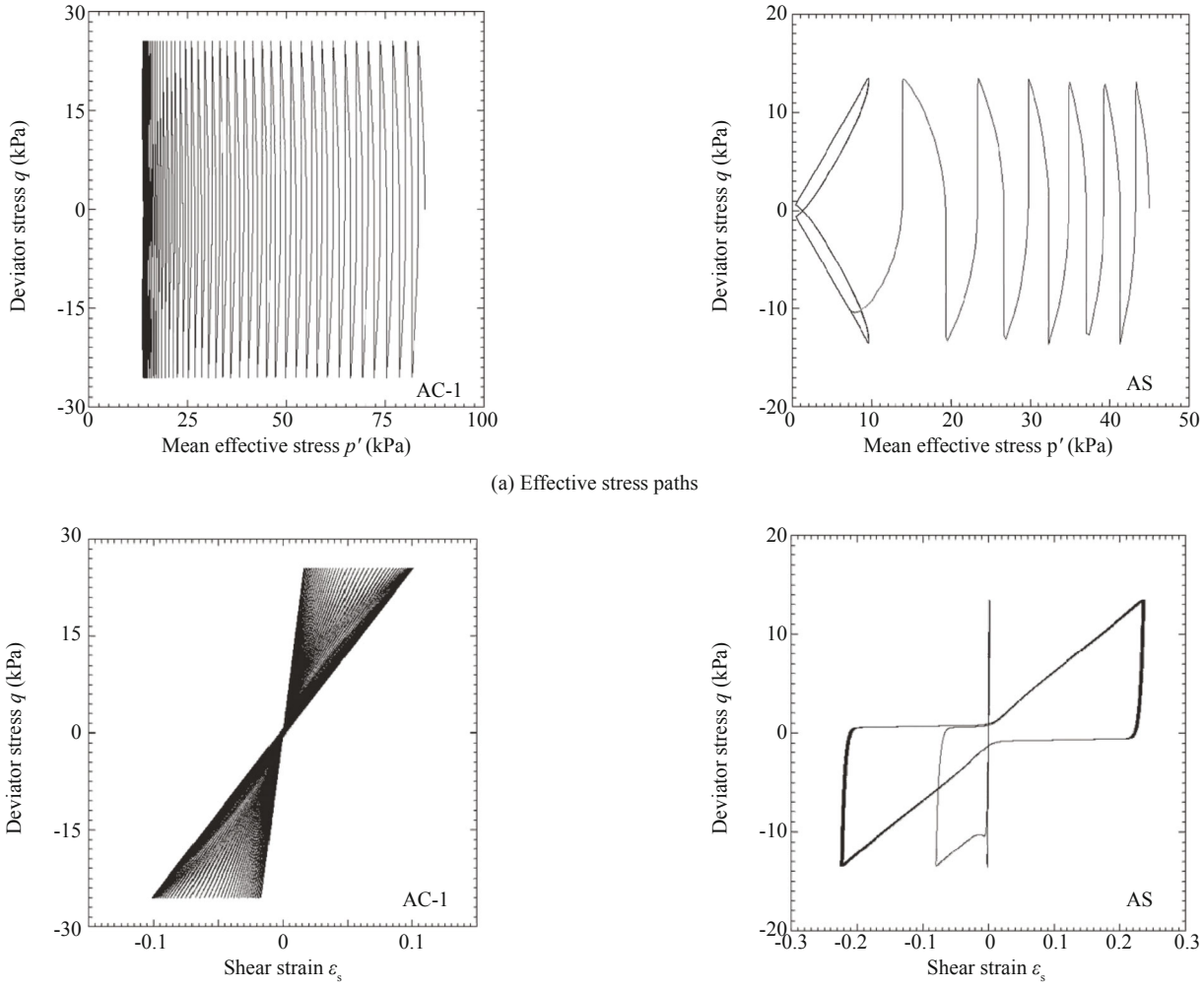

Fig. 7 Element behavior of some soils at Breakwater N site in cyclic triaxial tests under undrained conditions

required for complete dissipation of EPWP) after the earthquakes are discussed. Figure 9 shows the settlements at different points along the vertical lines A, B, and C in the case of Breakwater N during earthquake loadings. The soil beneath the breakwater (A1) settled continuously, whereas the soil 24 meters away from the breakwater (B1) heaved during the earthquake shaking, showing a typical sliding failure arc due to the breakwater's compatible deformation (Fig. 11a). The values of the settlements at point A1 reached 0.40 m in Case 1 and 0.25 m in Case 2 at the end of the earthquakes.

Figure 10 shows the settlements at different points along the vertical lines A, B, and C in the case of Breakwater N within sixty-eight years. Although the sandy surface liquefied during the earthquakes, points A1, B1, C1, A2, B2, and C2 settled continuously during the dissipation of EPWP and the values of settlements at point A1 reached 0.75 m in Case 1, and 0.6 m in Case 2 after sixty-eight years' consolidation.

Figure 11 shows the displacement vectors of Breakwater N and the foundation soil at the end of the earthquakes and sixty-eight years after the earthquakes. These vectors indicate that, due to the asymmetrical soil profiles on the right and left sides, the breakwater moved to the left with a maximum displacement increasing to 1.95 m. This asymmetrical deformation pattern occurred because the non-liquefied soil layer Ac-2 resisted further deformation on the right side, forcing the breakwater to move to the left.

Figure 12 shows the settlements distribution along three vertical lines at the time of sixty-eight years after the earthquakes. The largest settlements were 0.75 m in Case 1 and 0.6 m in Case 2. The settlement along vertical line A was the largest followed by vertical lines B and C. In other words, the largest settlement occurred directly beneath Breakwater N (vertical line A) after seismic excitations. The distribution of the settlements caused by these two earthquakes was similar, with the only exception being at the surface, where there was a prominent difference in the settlement.

4.2 Displacement of Breakwater C

The soil profiles of Breakwater C were more complicated than that of Breakwater N: there were 11 different soil layers beneath Breakwater C. The clayey

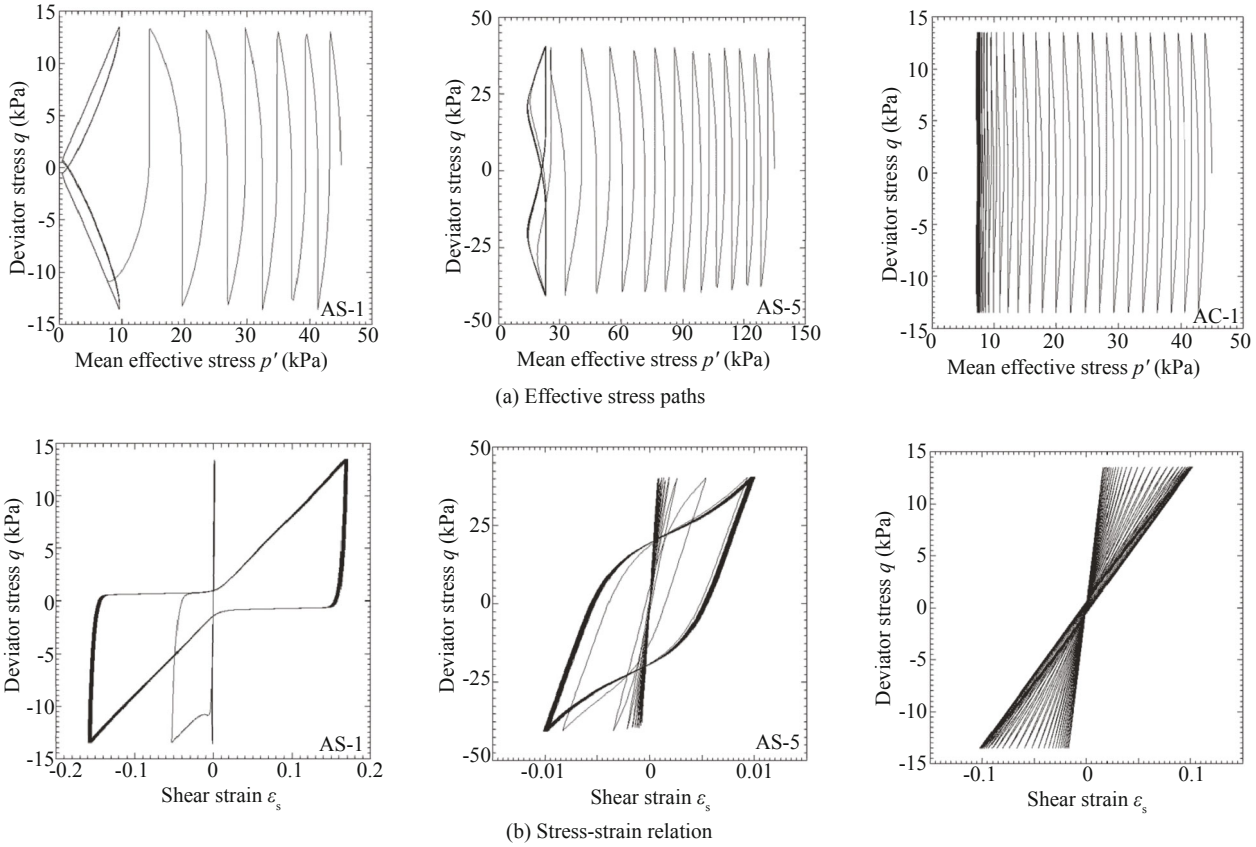

Fig. 8 Element behavior of some soils at Breakwater C site in cyclic triaxial tests under undrained conditions

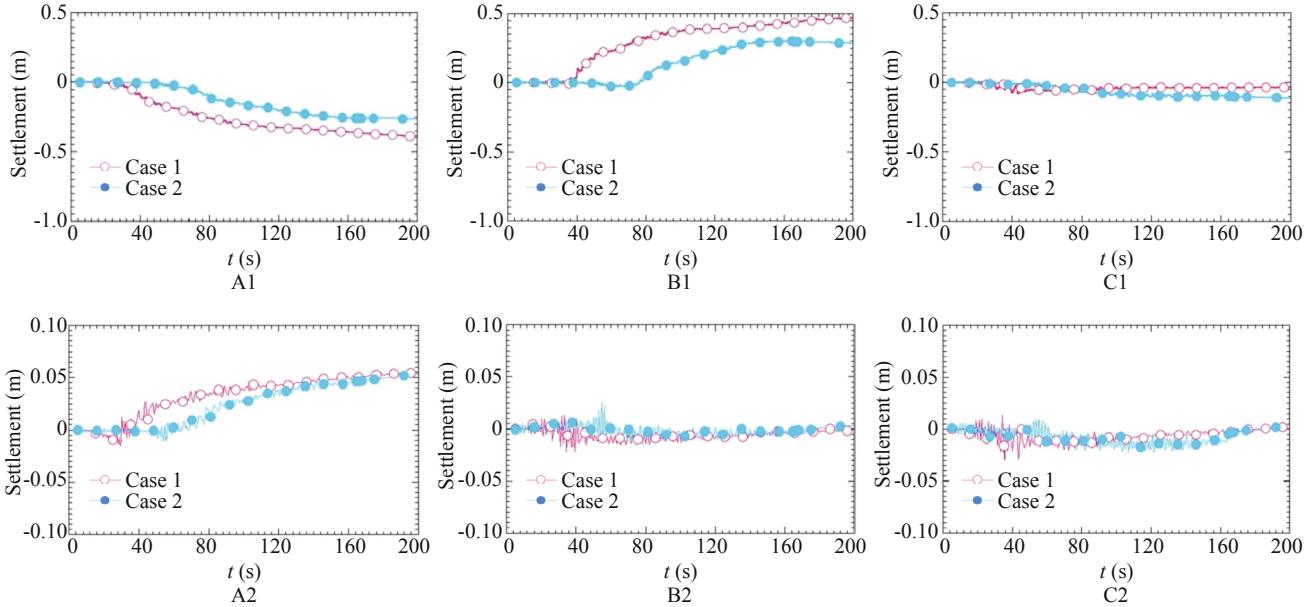

Fig. 9 Changes in settlements at prescribed points during the earthquake (Breakwater N)

layer directly beneath Breakwater C was replaced with sand, upon which the breakwater was laid. As shown in Figure 13, the sand at point A1 liquefied and settled to approximately 0.58 m in Case 1 and 0.40 m in Case 2 after the seismic loadings. After fifteen years (time required for completely dissipation of EPWP), it settled to approximately 0.80 m in Case 1 and 0.65 m in Case 2. In addition, the soil at B2 (Ac-2) heaved approximately 0.08 m in Case 1 and 0.02 m in Case 2 due to the compatible deformation of the breakwater after the earthquake, as it did in the case of Breakwater N. Because the clayey layers beneath Breakwater C

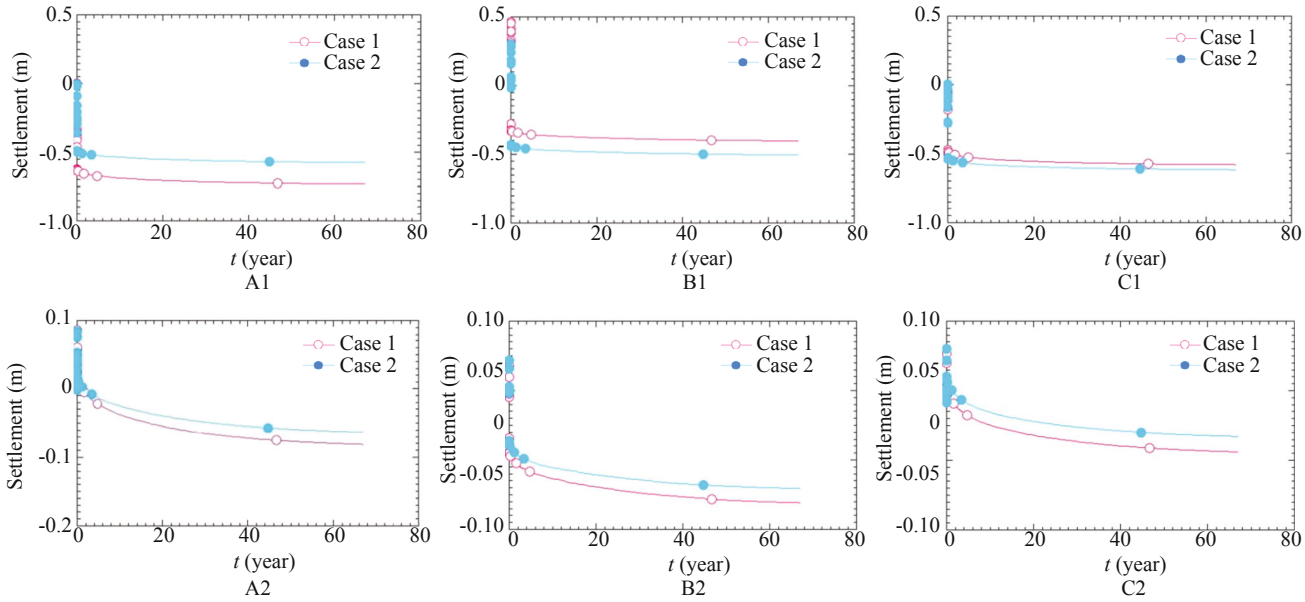

Fig. 10 Changes in settlements at prescribed points within sixty-eight years (Breakwater N)

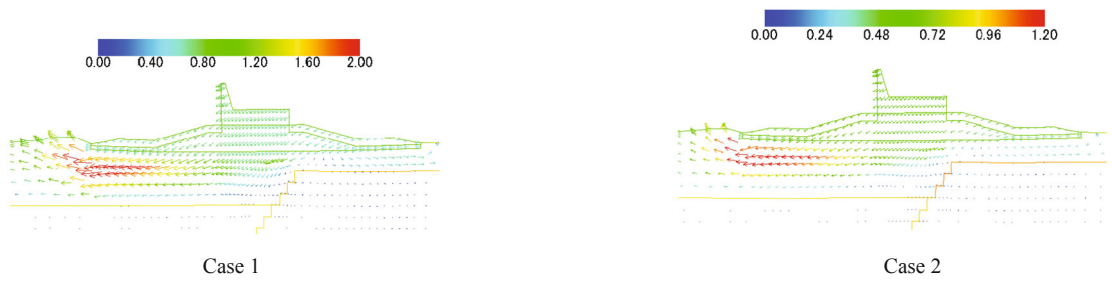

(a) End of earthquake motion (Unit: m)

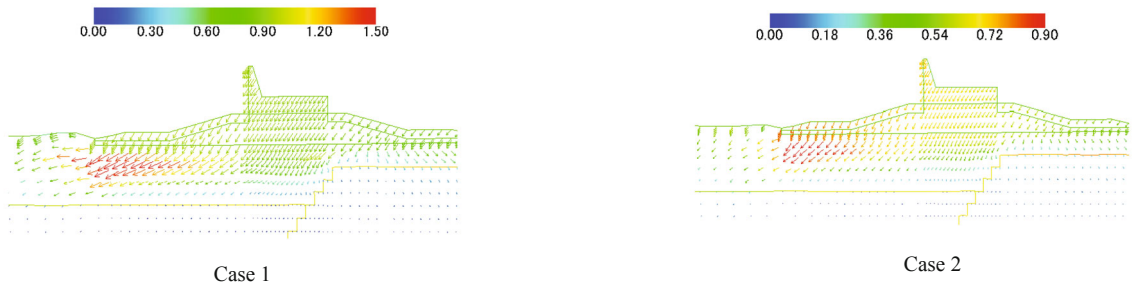

(b) Sixty-eight years after the earthquake (Unit: m)

Fig. 11 Displacement vectors of Breakwater N

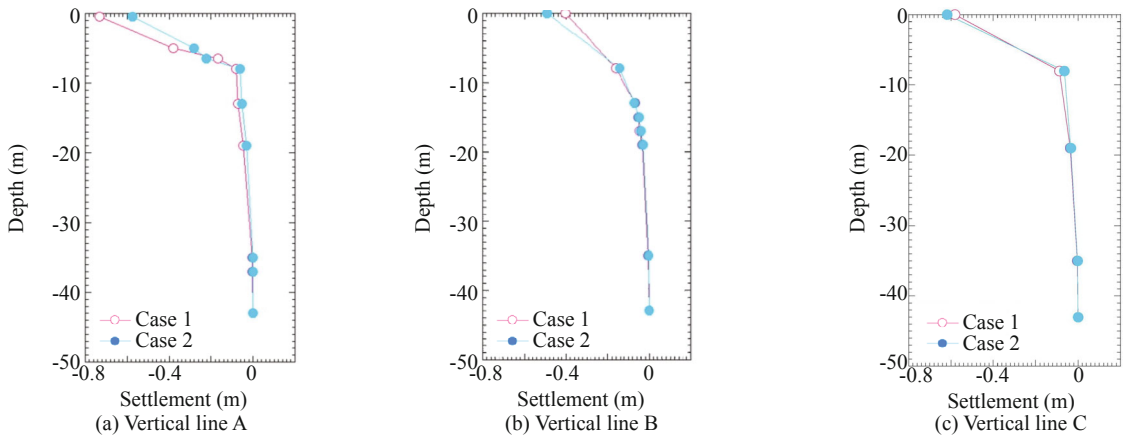

Fig. 12 Distribution of settlements sixty-eight years after the earthquake (Breakwater N)

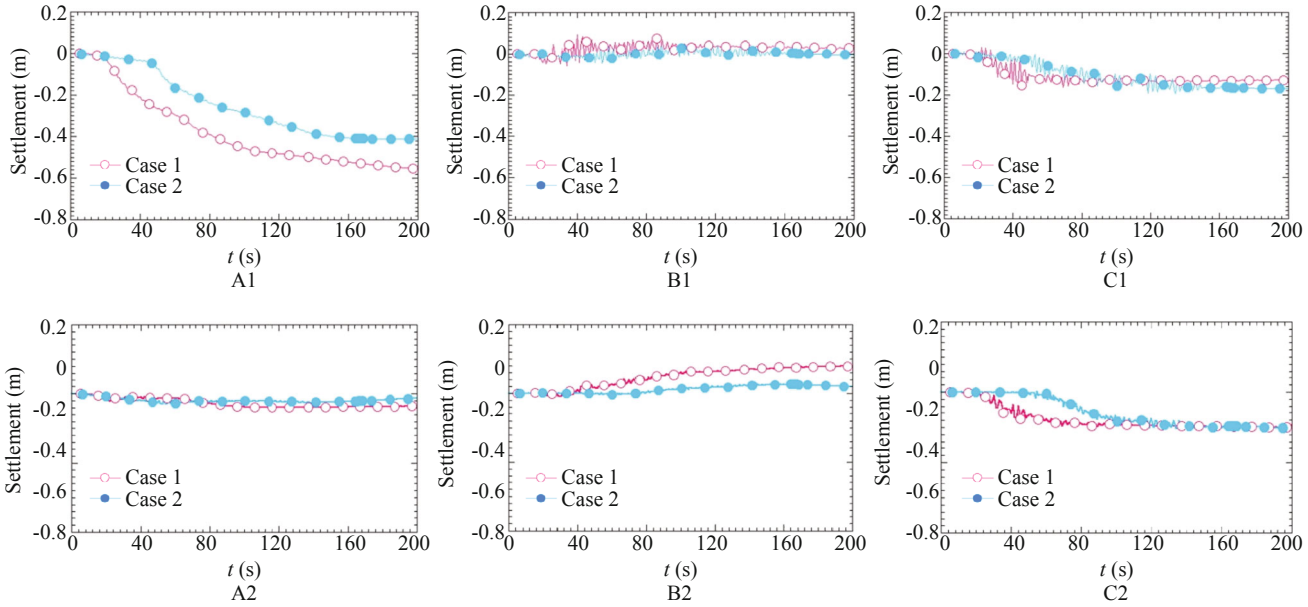

Fig. 13 Changes in settlements at prescribed points during the earthquake (Breakwater C)

were thinner than those beneath Breakwater N, the time required for completing EPWP dissipation was much shorter than that required for Breakwater N, and the settlement stopped at fifteen years after the earthquakes, as shown in Fig. 14.

Figure 15 shows the displacement vectors of Breakwater C and the foundation soil at the end of the earthquakes and fifteen years after the earthquakes. Different from the case in Breakwater N, the displacement vectors of Breakwater C showed a typical symmetrical sliding arc on both sides. The figure also shows that the settlement due to the dissipation of EPWP kept increasing for a long time, but lateral displacement stopped progressing soon after the earthquakes, as it did in Breakwater N. Figure 16 shows the distribution of settlements fifteen years after the earthquake along three vertical lines. Apparently, the settlement near the ground surface along vertical line A showed a larger value than that in the other locations near the ground surface; however, in deep places, the amount of settlement along vertical line C was greater than that in the other locations.

4.3 Brief summary of displacement

The amounts of settlements directly beneath the breakwaters at different times are listed in Table 10. In Breakwater N, the settlements at the end of the earthquakes were 0.40 m in Case 1 and 0.25 m in Case 2. In Breakwater C, the settlements at the end of the

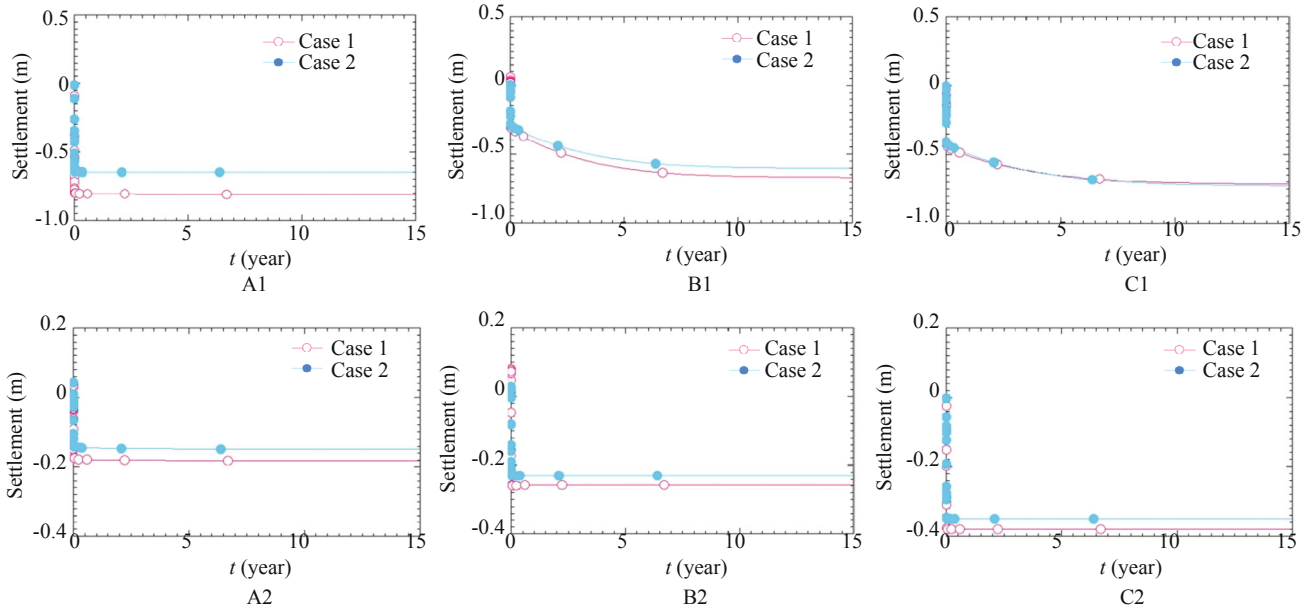

Fig. 14 Changes in settlements at prescribed points within fifteen years (Breakwater C)

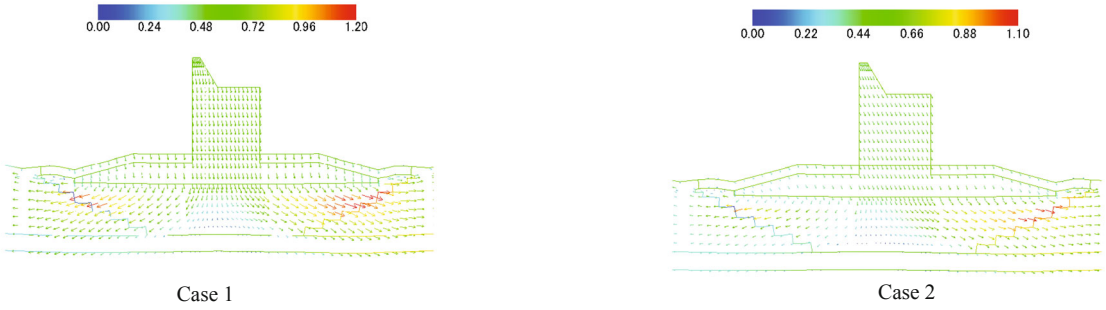

(a) End of earthquake motion (Unit: m)

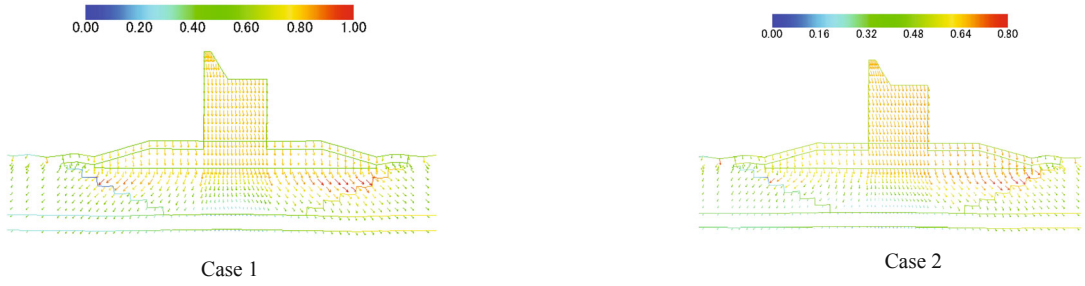

(b) Fifteen years after the earthquake (Unit: m)

Fig. 15 Displacement vectors of Breakwater C

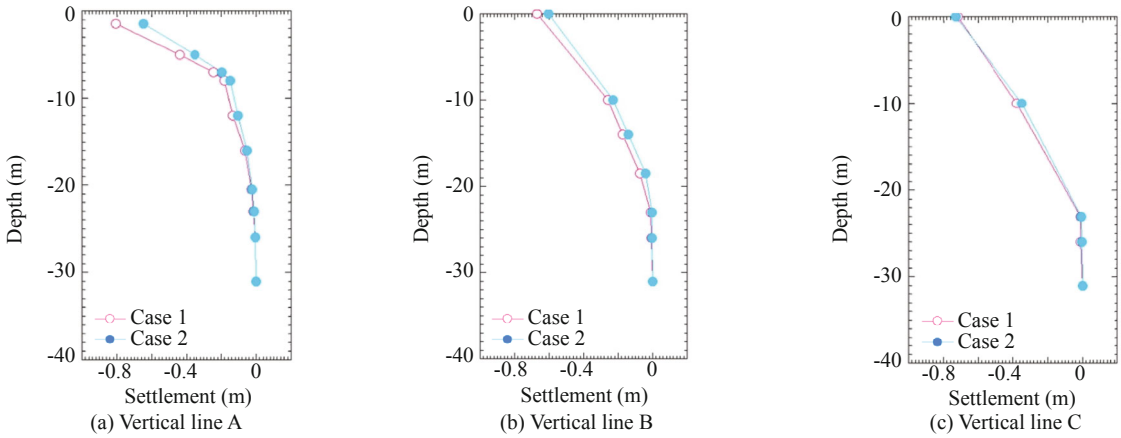

(a) Vertical line A (b) Vertical line B (c) Vertical line C

Fig. 16 Distribution of settlements fifteen years after the earthquake (Breakwater C)

Table 10 Settlements right beneath the breakwaters (Unit: m)

Time after earthquakes	Breakwater N		Breakwater C	
	Case 1	Case 2	Case 1	Case 2
0 second	-0.40	-0.25	-0.58	-0.40
1 hour	-0.60	-0.45	-0.65	-0.52
5 years	-0.68	-0.55	-0.80	-0.70
15 years	-0.70	-0.56	-0.80	-0.70
68 years	-0.71	-0.58		

earthquakes were 0.58 m in Case 1 and 0.40 m in Case 2. Because the duration and maximum acceleration of the earthquake in Case 1 was larger than that in Case 2, the settlement in Case 1 was greater than the one in Case 2. The settlement that occurs at the end of an earthquake is known as the compatible deformation. This deformation continued to increase to an overall settlement whose magnitude reached approximately 0.60-0.65 m within one hour after the earthquakes. The settlement of Breakwater C lasted approximately five years, whereas in Breakwater N, it lasted sixty-eight years due to the differences in the thicknesses of the clayey layers.

Generally speaking, a large tsunami reaches the shore within one hour after an earthquake. As shown in Table 10, the two breakwaters lost approximately more than half a meter of the height by this time due to the liquefaction-induced compatible deformation and overall settlement, which greatly reduced their capacity to resist the tsunami loading.

4.4 ESRR of Breakwater N

It is known that when sandy soil liquefies, EPWP increases while the effective stress decreases. The change in effective stress can be expressed by the effective stress reduction radio (ESRR), defined as $ESRR = 1\text{-}\sigma_m/\sigma_{m0}$, in which σ_m and σ_{m0} denote the current and initial mean effective stresses, respectively.

Figures 17 and 18 show the changes in ESRR during the seismic loading and sixty-eight years after the earthquakes, respectively, at elements A1, B1, and C1; these values increased to 1.0 during the earthquakes, implying that the topsoil under Breakwater N had liquefied completely. After the post-liquefaction consolidation, the ESRR decreased gradually and reached a certain steady values that were near but not equal to zero at sixty-eight years after the earthquakes, which implies that the effective stress did not return to its initial value due to its redistribution even when the EPWP had dissipated completely. The loss of mean effective stress during or shortly after an earthquake may have reduced the expected tsunami resistance capacity

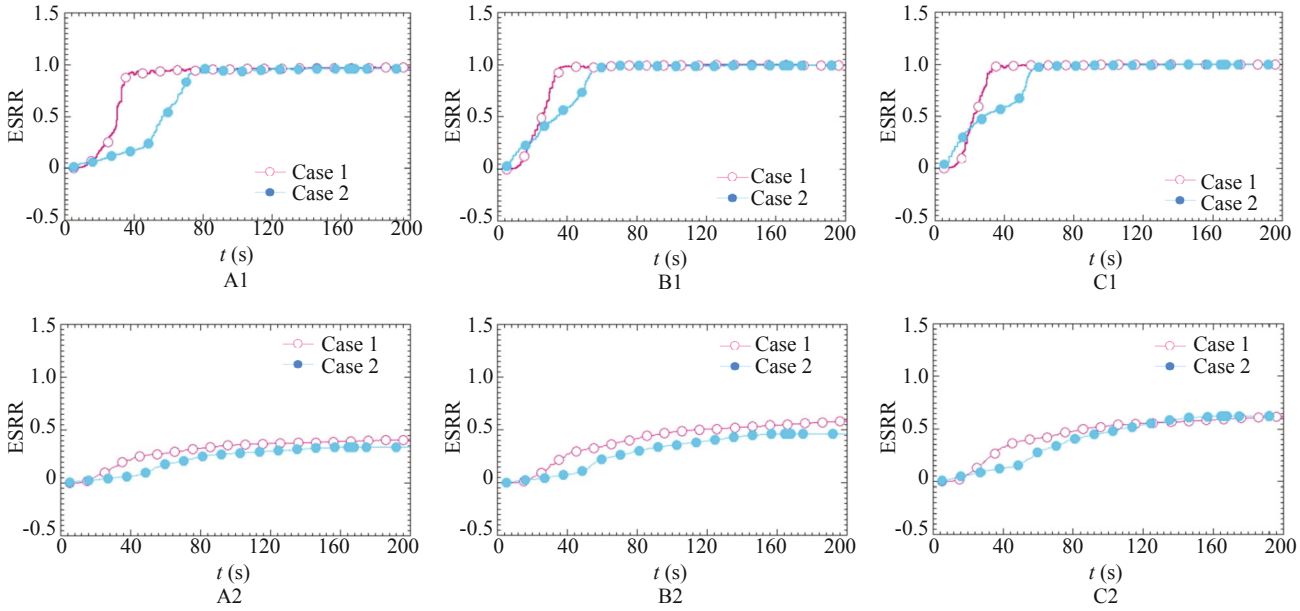

Fig. 17 Changes in ESRR at prescribed elements during the earthquake (Breakwater N)

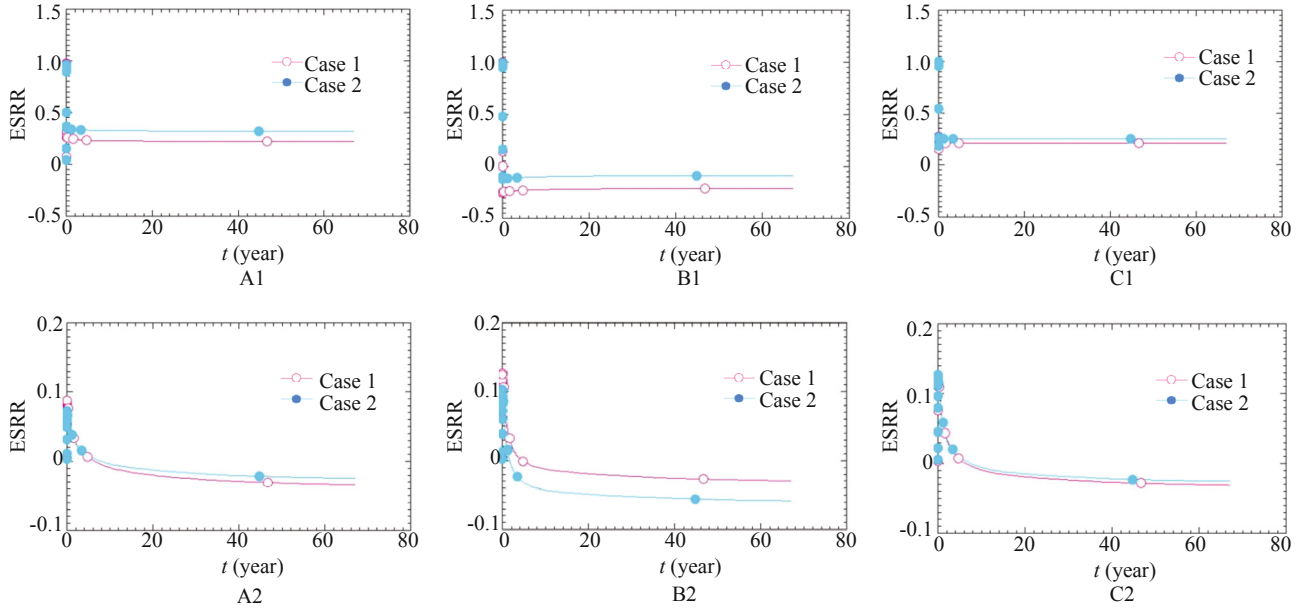

Fig. 18 Changes in ESRR at prescribed elements within sixty-eight years (Breakwater N)

of the breakwater from its initial design. On the other hand, the soils located at elements A2, B2, and C2 did not liquefy. The ESRR only increased to approximately 0.10, and the effective stress recovered completely in sixty-eight years.

4.5 ESRR of Breakwater C

As shown in Fig. 19, the ESRR at locations A1 (replaced sand As-1), B2 (sand layer As-2), and C2 (sand layer As-3) increased to 1.0 (completely liquefied), and the effective stress at these sites recovered in fifteen years, as shown in Fig. 20 due to changes in ESRR. By contrast, the ESRR at elements B1 and C1 (clayey layer Ac-1) decreased to 0.5 (and did not liquefy) during the earthquakes and became negative fifteen years after earthquakes, implying that the mean effective stress of the soil not only recovered but was also enhanced. The time to complete the dissipation of EPWP was approximately fifteen years, which is much shorter than in the case of Breakwater N, which required sixty-eight years.

4.6 Brief summary of ESRR

Table 11 lists the values of ESRR directly beneath the two breakwaters at different times. These values can also be used to describe changes in the effective stress. The soils beneath the two breakwaters liquefied completely during the earthquakes, but the degrees of recovery of

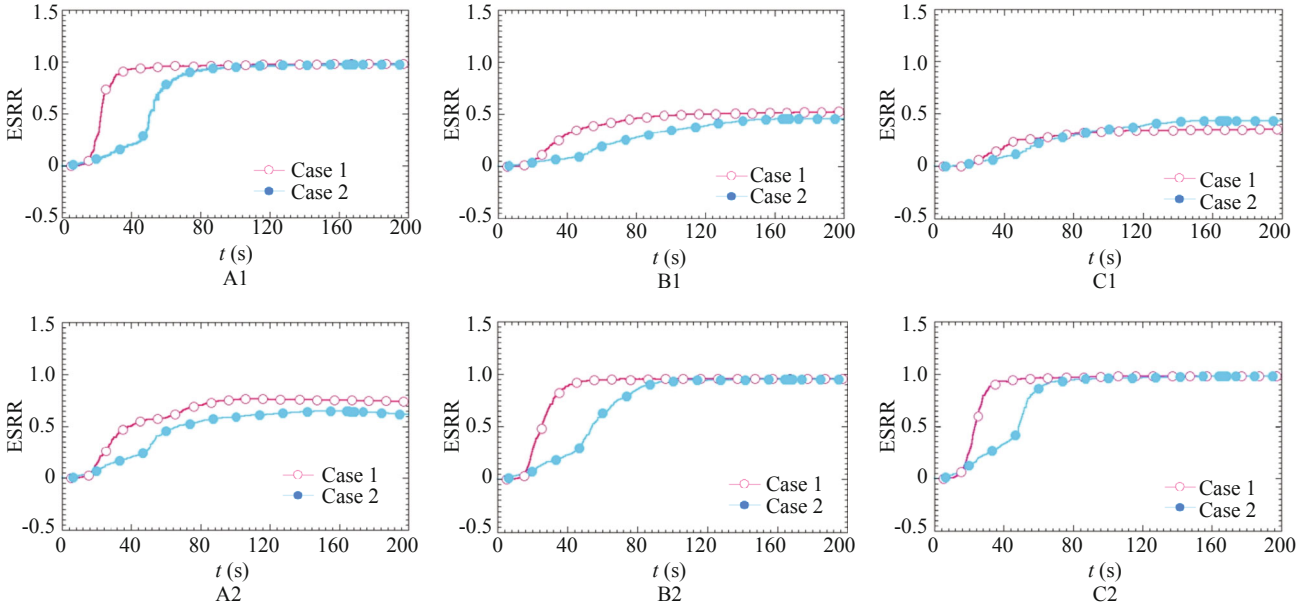

Fig. 19 Changes in ESRR at prescribed elements during the earthquake (Breakwater C)

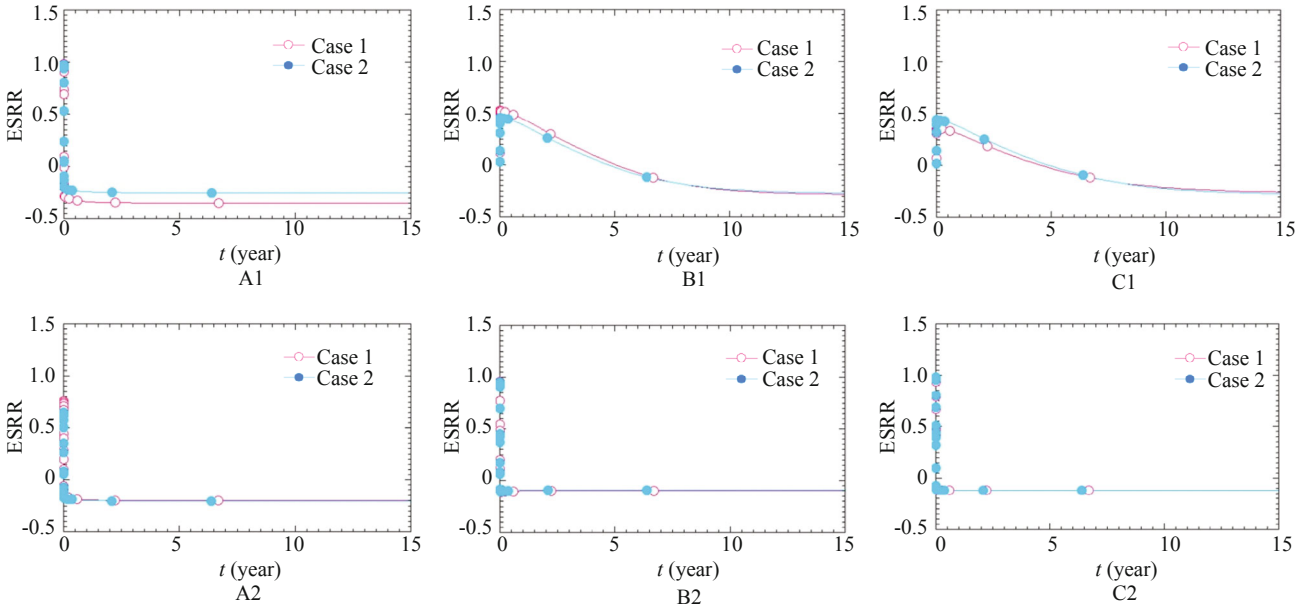

Fig. 20 Changes in ESRR at prescribed elements within fifteen years (Breakwater C)

Table 11 Values of ESRR right beneath the breakwaters

Time after earthquakes	Breakwater N		Breakwater C	
	Case 1	Case 2	Case 1	Case 2
0 second	1.0	1.0	1.0	1.0
1 hour	0.55	0.60	0.20	0.20
5 years	0.23	0.35	-0.20	-0.25
15 years	0.23	0.35	-0.20	-0.25
68 years	0.23	0.35		

the effective stress within one hour after the earthquakes were quite different: 40% (ESRR=60%) in Breakwater N, which had thick clayey layers beneath the liquefied soil, and 80% (ESRR=20%) in Breakwater C, which had sandy layers beneath the liquefied soil. Therefore, it can be first concluded that, from the perspective of tsunami resistance, seabed ground with thick clayey layers beneath liquefied soil are more vulnerable than seabed ground with only sandy layers from the results of effective stress recovery degree one hour after the earthquakes, which is the time that the tsunami is most likely to strike offshore structures. In other words, the slow speed of the effective stress recovery in seabed ground with thick clayey layers beneath liquefied soil could bring more risk for the breakwater to resist tsunami loading that may arrive a short time after earthquake shaking. This conclusion is quite different from the classical viewpoint that liquefaction only needs to be considered in sandy soils. Precautions should be taken when considering the tsunami resistance of a seabed ground whose soil profiles have a mixture of sandy and clayey layers. In normal seismic design (based on the classical viewpoint), liquefaction is only considered for loose sand in shallow soil layers (depth less than 15 m). Attention should also be given to the soil-water coupling behavior of clayey soils, which are impervious and can generate high EPWP when subjected to cyclic loadings.

5 Conclusions

Numerical tests were carried out to study the seismic behavior of seabed ground and the anti-tsunami performance of two existing breakwaters constructed forty years ago. It has been clearly illustrated that, in a normal numerical analysis of a practical geotechnical problem, the parameters of the soils involved in a prescribed constitutive model are adjusted to fit the observed behavior of a boundary value problem (BVP). In a numerical test, however, all of the soil parameters are determined based on element tests or engineering judgments without being influenced or modified by the observed behavior of a BVP. The final goal of a numerical test is not only to be able to simulate an actual event but also to predict an event that has not yet occurred when there is only part of the test data or the available information about the soils and some of the parameters are from element tests. The numerical tests were based on a sophisticated constitutive model that could describe the mechanical behavior of different soft soils at the element level in a unified way. Moreover, the corresponding soil-water coupling finite element analysis allowed the static and dynamic behavior of the boundary value problem to be treated in a unified way as well. The validity of this numerical method has been proved multiple times in the literature. From the results of numerical tests, the following conclusions can be drawn:

(1) After the earthquakes, the two breakwaters settled continuously due to the dissipation of pore water pressure and soil consolidation. The settlement of the ground was caused not only by the liquefied sandy soils but also by the clayey soils. The settlement at the end of the earthquake (local compatible deformation) was approximately 0.40-0.6 m, and the overall settlement was approximately 0.60-0.65 m one hour after the earthquakes. Generally speaking, each breakwater lost more than half a meter of height due to the liquefaction-induced compatible deformation and post-liquefaction consolidation. Meanwhile, the effective stress of the soils decreased greatly in the hour following the earthquakes. This means that the anti-tsunami capacity of the breakwaters had been weakened, which should be considered when evaluating the capacity of the breakwaters to resistance the subsequent tsunami loading.

(2) The settlement in Breakwater C lasted for approximately fifteen years and in Breakwater N lasted for sixty-eight years due to the different thicknesses of the clayey layers. This means that the thickness of the clayey layers greatly affects the time necessary for post-earthquake settlement, and that earthquakes affect not only the immediate behavior of breakwaters and their surrounding soils but also their long-term behavior due to post-earthquake consolidation.

(3) The deformation that occurs during an earthquake can be regarded as an undrained deformation in which a typical sliding arc forms in the ground, as in a static bearing capacity problem. Post-earthquake deformation, however, is a partially drained deformation in which mainly vertical settlement throughout the ground continues for a long time. Progression of the lateral displacement of both breakwaters stopped shortly after the earthquakes.

(4) From the perspective of tsunami resistance, a soil

profile with thick clayey layers beneath liquefied soil is more vulnerable than a soil profile with only sandy layers considering the slow speed of effective stress recovery that could bring more risk for breakwater when resisting the tsunami loading which may arrive a short time after earthquake shaking.

(5) Settlements which occurred during the earthquake shaking and in the post-liquefaction consolidation process can be calculated in a unified way because in the calculations, it is not necessary to predetermine whether each soil layer would liquefy or not. This approach differs from the traditional method in which only sand is considered in the liquefaction analysis and the liquefaction and post-liquefaction consolidation processes are treated in different ways; for instance, by using different values of parameters in different loading stages.

Acknowledgment

This work was supported by the National Natural Science Foundation of China (Grant Nos. 51678369, 41627801 and 41372284), Technical Innovation Foundation of Shenzhen (Grant No. JCYJ20170302143610976), Doctoral Fund of Shandong Province (Grant No. ZR2017BEE071), China Postdoctoral Science Foundation (Grant No. 2017M612227) and the Special Project Fund of Taishan Scholars of Shandong Province (Grant No. 2015-212).

References

Asaoka A, Noda T, Yamada E, Kaneda K and Nakano M (2002), "An Elasto-Plastic Description of Two Distinct Volume Change Mechanisms of Soils," *Soils and Foundations* , **42**(5): 47–57.

Asaoka A (2003), "Consolidation of Clay and Compaction of Sand -An Elasto-Plastic Description," *Proc. 12th Asian Regional Conference on SMGE*, Keynote paper, Singapore, **2**: 1157–1195.

Biot MA (1941), "General Theory of Three-Dimensional Consolidation," *Journal of Applied Physics.* **12**(2): 155–164.

Bao XH, Morikawa Y, Kondo Y and Nakamura K (2012), "Shaking Table Test on Reinforcement Effect of Partial Ground Improvement for Group-Pile Foundation and Its Numerical Simulation," *Soils and Foundations*, **52**(6): 1043–1061.

Bao XH, Ye GL, Ye B, Sago Y and Zhang F (2014), "Seismic Performance of SSPQ Retaining Wall-Centrifuge Model Tests and Numerical Evaluation," *Soil Dynamics and Earthquake Engineering*, **61**(62): 63–82.

Bao XH, Ye B, Ye GL and Zhang F (2016), "Co-Seismic and Post-Seismic Behavior of a Wall Type Breakwater on a Natural Ground Composed of Liquefiable Layer, " *Natural Hazards*, **83**(3): 1799–1819.

Central Disaster Management Council (CDMC), Cabinet Office, Government of Japan, http://www.bousai.go.jp/1info/pdf/saigaipanf_e.pdf.

Furuta, R (2003), "Modeling of Dynamic Behavior of Multi-Layered Ground and Its Application to Earthquake Engineering," *Doctoral Dissertation*, Gifu University.

Hashiguchi K and Ueno M (1977), "Elastoplastic Constitutive Laws of Granular Material," Constitutive Equations of Soils. Proc. 9th Int. Conf. Soil Mech. Found. Engrg., Spec. Ses. 9, Murayama, S. and Schofield, A. N. (eds.); Tokyo, JSSMFE, 73–82.

Huang Y and Jiang XM (2010), "Field-Observed Phenomena of Seismic Liquefaction and Subsidence during the 2008 Wenchuan Earthquake," *Natural Hazards*, **54**(3): 839–850.

Huang Y, Zheng H and Zhuang ZJ (2012), "Seismic Liquefaction Analysis of Reservoir Dam Foundation in the South-North Water Diversion Project in China. Part II: Seismic Response Simulation," *Natural Hazards*, **60**: 1313–1324.

Hur DS, Kim CH and Yoon JS (2010), "Numerical Study on the Interaction Among a Nonlinear Wave, Composite Breakwater and Sandy Seabed," *Coastal Engineering*, **57**: 917–930.

Imase T, Maeda K, Miyake M, Sawada Y, Tsurugasaki K, Sumida H and Zhang F (2012), "Destruction of Caisson-Type Breakwater due to Bearing Capacity by Tsunami with Seabed Soil Damage by Earthquake and Overflow," Journal of JSCE, **68**(2): I886–I870. (in Japanese)

Morikawa Y (2013), "Clarification of the Mechanism of Re-Liquefaction and Its Application to Evaluate Seismic Enhancement Effect of Various Kinds of Ground Improvement," *Doctoral dissertation of Nagoya Institute of Technology*. (in Japanese)

Novikova T, Papadopoulos GA and Karastathis V (2007), "Evaluation of Ground Motion Characteristics, Effects of Local Geology and Liquefaction Susceptibility: the Case of Itea, Corinth Gulf (Greece)," *Natural Hazards*, **40**(3): 537–552.

Pastor, M, Zienkiewicz, OC and Chan AHC (1990), "Generalized Plasticity and the Modelling of Soil Behaviour," *Int J Numer Anal Methods Geomech*, **14**: 151–90.

Sawicki A and Mierczynski J (2009), "On the Behavior of Liquefied Soil," *Computers and Geotechnics*, **36**: 531–536.

Sugito *et al*. (2013), "Website of Earthquake Disaster Prevention Information," Gifu University, http://www1.gifu-u.ac.jp/~eerl/kensaku/index.html. (in Japanese)

Wang ZL, Dafalias YF and Shen CK (1990), "Bounding Surface Hypoplasticity Model for Sand", *Journal of Engineering Mechanics*, **116**(5): 983–1001.

Wang G and Xie Y (2014), "Modified Bounding Surface Hypoplasticity Model for Sands under Cyclic Loading", *Journal of Engineering Mechanics*, **140**(1): 91–104.

Wang MW, Chen GY and Iai S (2013), "Seismic Performances of Dyke on Liquefiable Soils," *Journal of Rock Mechanics and Geotechnical Engineering*, **5**: 294–305.

Ye JH and Wang G (2015), "Seismic Dynamics of Offshore Breakwater on Liquefiable Seabed Foundation," *Soil Dynamics and Earthquake Engineering*, **76**: 86–99.

Ye JH, Huang D and Wang G (2016), "Nonlinear Simulation of Offshore Breakwater on Sloping Liquefied Seabed," *Bulletin of Engineering Geology and the Environment*, **75**: 1215–1225.

Yen H, Sato S and Tajima Y (2013), "The 11th March 2011 East Japan Earthquake and Tsunami, Tsunami Effects on Coastal Infrastructure and Buildings," *Geophysics*, **170**: 1019–1031.

Ye GL, Sheng JR, Ye B and Wang JH (2012), "Automated True Triaxial Apparatus and Its Application to Over-Consolidated Clay," *Geotechnical Testing Journal*, **35**(4): 517–528.

Ye GL, Ye B and Zhang F (2013), "Strength and Dilatancy of Overconsolidated Clays in Drained True Triaxial Tests," *Journal of Geotechnical and Geo-Environmental Engineering*, **140**(4): 06013006.

Ye B, Ye GL and Zhang F (2012), "Numerical Modeling of Changes in Anisotropy During Liquefaction Using a Generalized Constitutive Model," *Computers and Geotechnics*, **42**: 62–72.

Ye B, Ye GL, Zhang F and Yashima A (2007), "Experiment and Numerical Simulation of Repeated Liquefaction-Consolidation of Sand," *Soils and Foundations*, **47**(3): 547–558.

Ye B (2007), "Experiment and Numerical Simulation of Repeated Liquefaction-Consolidation of Sand," *Doctoral Dissertation*, Gifu University.

Zhang F, Ye B, Noda T, Nakano M and Nakai K (2007), "Explanation of Cyclic Mobility of Soils: Approach by Stress-Induced Anisotropy," *Soils and Foundations*, **47**(4): 635–648.

Zhang F, Ye B and Ye GL (2011), "Unified Description of Sand Behavior," *International Journal of Frontiers of Structure and Civil Engineering*, **5**(2): 121–150.